

# Abrikosov Vortices in Type II Superconductors

Emma Batson  
 EECS  
 emmabat@mit.edu

Matteo Castellani  
 EECS  
 mcaste@mit.edu

Owen Medeiros  
 EECS  
 omedeiro@mit.edu

**Abstract**—Type II superconductors are a promising platform for many kinds of electronics, providing low losses and high nonlinearities with many applications. However, the materials physics of superconducting devices, modeled by the Ginzburg-Landau theory, can be quite complex. In the presence of magnetic fields, cylindrical regions named Abrikosov vortices, where superconductivity is destroyed, can form within a type II superconductor. We simulate the generation of Abrikosov vortices in a 3-D geometry due to an external magnetic field, in order to better understand the behavior of superconducting devices.

## I. INTRODUCTION & MOTIVATIONS

Superconducting electronics exhibit zero resistivity and large nonlinearities of engineering interest. As such, they may be useful in situations requiring low loss or high sensitivity, such as computers on interstellar missions, or as detectors in powerful telescopes.

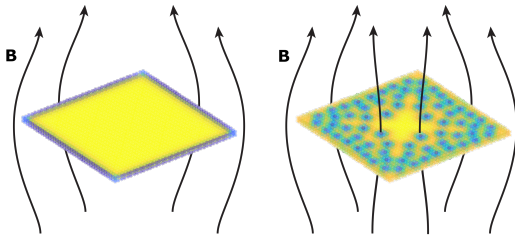


Fig. 1. A comparison of Type-I (left) and Type-II (right) superconductors under an applied magnetic field. Image obtained simulating a 60x60x3 grid. Yellow regions are superconducting. Blue regions are normal.

Normally, superconductors expel all magnetic field below a critical value, above which they return to normal state. However, type II superconductors have two critical magnetic field values. Below the first, they still expel all field. Above the second, they return to normal state. Between these two values, however, a type II superconductor will admit some field, resulting in localized destruction of superconductivity in Abrikosov vortices within the material. [2]

The dynamics of these vortices has several practical applications. In commercial applications, the magnetic fields that penetrate the superconductor (flux pinning) provide stability for maglev trains which have reached speeds approaching 600kph. [8] In academic research, beyond being an intriguing fundamental physics topic, vortex dynamics in superconducting single photon detectors contribute to detector latency. [3] Studying vortex dynamics will improve the development of single photon detectors, which impact fields ranging from biomedical imaging to deep space communication.

## II. PROBLEM FORMULATION

In a superconductor the current is carried by coupled electrons, called Cooper pairs, and the spatial density of pairs is given by the squared wavefunction  $|\psi|^2$ . The Ginzburg-Landau model describes the electromagnetic dynamics of a superconducting material as a function of  $\psi$ , the scalar potential  $\Phi$ , and the vector potential  $\mathbf{A}$ .

In accordance with the mathematical formulation from [7], the Ginzburg-Landau equations from [1] can be written in terms of only  $\psi$  and  $\mathbf{A}$ , preserving important physical properties of the system such as electromagnetic gauge invariance. The Ginzburg-Landau model in dimensionless units is described by equations 1 and 2.  $S$  is the complex phase of  $\psi$  and  $\kappa$  is the Ginzburg-Landau parameter.  $\psi$  is scaled in multiples of  $\psi_0 = \sqrt{|a|/b}$ , where  $a$  and  $b$  are material parameters.  $\mathbf{A}$  is scaled in multiples of  $\mathbf{A}_0 = \sqrt{2}\kappa\mathbf{H}_c\xi$ , where  $\mathbf{H}_c$  is the critical field and  $\xi$  is the coherence length, radius of Abrikosov vortices.  $t$  is scaled in multiples of  $\tau = \xi^2/\kappa^2$ .

$$\frac{\partial\psi}{\partial t} = (\nabla - i\mathbf{A})^2\psi + \psi - |\psi|^2\psi \quad (1)$$

$$\frac{\partial\mathbf{A}}{\partial t} = (\nabla S - \mathbf{A})|\psi|^2 - \kappa^2\nabla \times \nabla \times \mathbf{A} \quad (2)$$

We use equations 1 and 2 to model a 3-D block of superconducting material, which is discretized in a  $(N_x - 1) \times (N_y - 1) \times (N_z - 1)$  network. The block is surrounded by one layer of vacuum, where a magnetic field  $\mathbf{B}$  is applied. The nodes are the  $\psi$  at each point in the network. The branches couple the nodes with a strength determined by the value of  $\mathbf{A}$  in close proximity of the node.

### A. State Vector

When discretizing, the  $\mathbf{A}$  gauge invariance is not preserved in general. In order to maintain gauge invariance a complex link variable  $U_i^x = \exp(-i\phi_i^x)$  is defined for each branch, where  $\phi_i^x = \int_{x_i}^{x_{i+1}} \mathbf{A}(x')dx'$ . Branch and nodes variables are not separable, so the state vector for  $N = (N_x - 1)(N_y - 1)(N_z - 1)$  nodes and  $N' = (N_x - 2)(N_y - 2)(N_z - 2)$  branches is:

$$x = [\psi_1 \ \psi_2 \dots \psi_N \ \phi_1^x \ \phi_2^x \dots \phi_{N'}^x \ \phi_1^y \ \phi_2^y \dots \phi_{N'}^y \ \phi_1^z \ \phi_2^z \dots \phi_{N'}^z]^T \quad (3)$$

Where  $m = i + j(N_x - 1) + k(N_x - 1)(N_y - 1)$ ,  $\psi_{i,j,k} = \psi_m$ .

## B. Parameters

The equations used in our state space are dimensionless. The remaining parameters are the Ginzburg-Landau parameter,  $\kappa = (2m^2b)/(e^2\hbar^2\mu_0)$ , the spacial discretization lengths,  $h_x$ ,  $h_y$ ,  $h_z$ , and the number of nodes,  $N_x$ ,  $N_y$ ,  $N_z$ . If  $\kappa > 1/\sqrt{2}$  the material acts like a type II superconductor, otherwise as a type I superconductor. We allow for modeling geometries with periodic boundary conditions along selected directions. This is encoded with parameters  $d_x$ ,  $d_y$ ,  $d_z$ , which are 1 when the associated direction is periodic and 0 when it is not.

$$p = [\kappa \ h_x \ h_y \ h_z \ N_x \ N_y \ N_z \ d_x \ d_y \ d_z]^T \quad (4)$$

## C. Inputs

Vortices are formed by applying a magnetic field  $\mathbf{B}$  on the boundaries of the block. An extra layer of  $\phi$  and  $\psi$ , not considered in  $x$  is added on the boundaries to model the external applied field in vacuum. The inputs of the system are the values of  $B_n^x$ ,  $B_n^y$ , and  $B_n^z$  in each 3D box  $n$  formed by nearest neighbours  $\phi$  at the boundaries with the vacuum layer.  $B_n^x$  depends on  $\phi$  as shown in equation 13, so it is possible to define the relevant boundary conditions for  $\phi$ . The input vector for  $N'' = 2(N_x - 2)(N_y - 2) + 2(N_x - 2)(N_z - 2) + 2(N_y - 2)(N_z - 2)$  is:

$$u = [B_1^x \ B_2^x \ \dots \ B_{N''}^x \ B_1^y \ B_2^y \ \dots \ B_{N''}^y \ B_1^z \ B_2^z \ \dots \ B_{N''}^z]^T \quad (5)$$

## D. Dynamical State Space System

A three dimensional discretized superconducting block is described by the following equations.

$$\frac{dx}{dt} = f(x, p, u) = \left[ \frac{\partial \psi}{\partial t} \ \frac{\partial \phi^x}{\partial t} \ \frac{\partial \phi^y}{\partial t} \ \frac{\partial \phi^z}{\partial t} \right]^T \quad (6)$$

$$\begin{aligned} \frac{\partial \psi_{i,j,k}}{\partial t} &= \frac{\overline{U}_{i-1,j,k}^x \psi_{i-1,j,k} - 2\psi_{i,j,k} + U_{i,j,k}^x \psi_{i+1,j,k}}{h_x^2} \\ &+ \frac{\overline{U}_{i,j-1,k}^y \psi_{i,j-1,k} - 2\psi_{i,j,k} + U_{i,j,k}^y \psi_{i,j+1,k}}{h_y^2} \\ &+ \frac{\overline{U}_{i,j,k-1}^z \psi_{i,j,k-1} - 2\psi_{i,j,k} + U_{i,j,k}^z \psi_{i,j,k+1}}{h_z^2} \\ &+ (1 - |\psi_{i,j,k}|^2)\psi_{i,j,k} \end{aligned} \quad (7)$$

$$\begin{aligned} \frac{\partial \phi_{i,j,k}^x}{\partial t} &= \frac{\kappa^2}{h_y^2}(\phi_{i,j-1,k}^x - 2\phi_{i,j,k}^x + \phi_{i,j+1,k}^x) \\ &+ \frac{\kappa^2}{h_z^2}(\phi_{i,j,k-1}^x - 2\phi_{i,j,k}^x + \phi_{i,j,k+1}^x) \\ &+ \frac{\kappa^2}{h_y^2}(-\phi_{i+1,j,k}^y + \phi_{i,j,k}^y + \phi_{i+1,j-1,k}^y - \phi_{i,j-1,k}^y) \\ &+ \frac{\kappa^2}{h_z^2}(-\phi_{i+1,j,k}^z + \phi_{i,j,k}^z + \phi_{i+1,j,k-1}^z - \phi_{i,j,k-1}^z) \\ &+ \text{Im}(\exp(-i\phi_{i,j,k}^x)\overline{\psi}_{i,j,k}\psi_{i+1,j,k}) \end{aligned} \quad (8)$$

Where  $U_{i,j,k}^x = \exp(-i\phi_{i,j,k}^x)$ . Equations for  $\frac{\partial \phi_{i,j,k}^y}{\partial t}$  and  $\frac{\partial \phi_{i,j,k}^z}{\partial t}$  can be obtained via cyclical permutation. Bar notation indicates conjugation  $\overline{\psi} \equiv \psi^*$ .

*1) Boundary Conditions:* The boundary conditions depends on the geometry of the system. In a three dimensional systems we can set either periodic boundary conditions or zero-current (“vacuum”) boundary conditions in  $x$ ,  $y$ , and  $z$ . For instance, if we are periodic in  $z$  and zero-current in  $x$  and  $y$ , we are simulating a periodic, infinitely long, square wire. In this case, through the length of the wire  $k = 1 : N_z + 1$  there are periodic boundary conditions.

$$\psi_{i,j,1} = \psi_{i,j,N_z}, \quad \psi_{i,j,2} = \psi_{i,j,N_z+1} \quad (9)$$

$$\phi_{i,j,1}^z = \phi_{i,j,N_z}^z, \quad \phi_{i,j,2}^z = \phi_{i,j,N_z+1}^z \quad (10)$$

Furthermore, along  $x$ - and  $y$ -directions there are conditions to ensure zero current flow at the boundaries.

$$\psi_{1,j,k} = \psi_{2,j,k} U_{1,j,k}^x, \quad \psi_{N_x+1,j,k} = \psi_{N_x,j,k} \bar{U}_{N_x,j,k}^x \quad (11)$$

$$\psi_{i,1,k} = \psi_{i,2,k} U_{i,1,k}^y, \quad \psi_{i,N_y+1,k} = \psi_{i,N_y,k} \bar{U}_{i,N_y+1,k}^y \quad (12)$$

Changing which dimensions have period or zero-current boundaries can be done similarly, with simple changes of indices.

## E. Outputs

Perhaps the most important output is  $|\psi(r, t)|^2$ , which indicates the superconducting state of the material as a function of position in time. Where this quantity is one, the material has fully superconducting behavior. Where it is zero, the system is in the normal state with no superconductivity. In-between values indicate degraded superconductivity. Inside a vortex  $|\psi(r)|^2 = 0$ , and it gradually becomes one moving away from the center.

We may also wish to examine the magnetic field of the system as a function of position in time,  $B(r, t)$ . This quantity is obtained from  $\phi$  using equation 13. Equations for  $B_{i,j,k}^y$ ,  $B_{i,j,k}^z$  are found by cyclic permutation.

$$B_{i,j,k}^x = \frac{1}{h_y h_z} (\phi_{i,j,k}^y - \phi_{i,j,k+1}^y - \phi_{i,j,k}^z - \phi_{i,j+1,k}^z) \quad (13)$$

The output vector is:

$$y = [| \psi_1 |^2 \ \dots \ | \psi_N |^2 \ B_1^x \dots B_{N'}^x \ B_1^y \dots B_{N'}^y \ B_1^z \dots B_{N'}^z]^T \quad (14)$$

## III. FUNDAMENTAL NUMERICAL METHODS

We consider what system response is of interest and then develop a suitable numerical method optimized to produce the desired output. For superconducting vortices, the steady state impulse, step or slowly varying input, response is of interest, as the creation and annihilation of vortices reveal microscopic dynamics that can produce potentially undesirable fluctuations in measured voltages or magnetic fields. To solve each time iteration a trapezoidal time integration method was developed. This method was preferred over a Forward or Backward Euler integrator due to the reduced error at large time steps. Within this integrator there are two nested algorithms (Newton-GCR,

TGCR) to return the change in our state variables over the time step. Reference Algorithms 1, 2, 3 for a description of each numerical procedure.

---

**Algorithm 1** Trapezoidal Integrator

---

**Require:**  $x(t^0) = x^0$   
**Ensure:**  $x$  is the solution of  $\frac{dx}{dt} = f(x, p, u)$

```

function TRAPEZOIDAL( $f(\cdot), x^0, p, u(\cdot), t^0, t^{end}, \Delta t$ )
     $n \leftarrow 0$ 
    repeat
         $n \leftarrow n + 1$ 
         $t^n \leftarrow t^{n-1} + \Delta t$ 
         $\hat{x}^n \leftarrow x^{n-1} + \Delta t \times f(x^{n-1}, p, u(t^{n-1}))$ 
         $\gamma \leftarrow x^{n-1} + \Delta t/2 \times f(x^{n-1}, p, u(t^{n-1}))$ 
         $x^n \leftarrow \text{NewtonGCR}(f(\cdot), \hat{x}^n, p, u(\cdot), t^{n-1}, \Delta t, \gamma)$ 
    until  $t^n \geq t^{end}$ 
    return  $[x^0 \ x^1 \ x^2 \dots x^n], [t^0 \ t^1 \ t^2 \dots t^n]$ 

```

---

**Algorithm 2** Newton-GCR

---

**Require:** maxError, maxIter the user's acceptable bounds for termination of Newton  
**Ensure:**  $x$  is the solution of  $0 = \hat{f}(x, p, u)$

```

function NEWTONGCR( $f(\cdot), x^0, p, u(\cdot), t, \Delta t, \gamma$ )
     $k \leftarrow 0$ 
    repeat
         $k \leftarrow k + 1$ 
         $\hat{f} \leftarrow x^{k-1} - \Delta t/2 \times f(x^{k-1}, p, u(t)) - \gamma$ 
         $\Delta x \leftarrow \text{TGCR}(f(\cdot), \hat{f}, x^{k-1}, p, u(\cdot), t, \Delta t)$ 
         $x^k \leftarrow x^{k-1} + \Delta x$ 
    until  $k > \text{maxIter} \text{ || } |f(x^k)|, |\Delta x| < \text{maxError}$ 
    return  $x^k$ 

```

---

**Algorithm 3** TGCR

---

**Require:**  $\hat{\epsilon}$  a perturbation sufficiently small for convergence  
**Ensure:**  $x$  is the solution of  $J_{\hat{f}}x = -\hat{f}(x^0, p, u)$

```

function TGCR( $f(\cdot), \hat{f}, x^0, p, u(\cdot), t, \Delta t$ )
     $k \leftarrow 0, r \leftarrow -\hat{f}$ 
    repeat
         $k \leftarrow k + 1, p \leftarrow r$ 
         $\epsilon \leftarrow \hat{\epsilon} \times (1 + |x^0|/|p|)$ 
         $A_{pk} \leftarrow p - \Delta t/2 \times (f(x^0 + \epsilon, u(t)) - f(x^0, u(t)))$ 
        Orthonormalize with Gram-Schmidt
         $\alpha \leftarrow r^T \times A_{pk}$ 
         $x \leftarrow x + \alpha \times p$ 
         $r \leftarrow r - \alpha \times A_{pk}$ 
    until  $k > \text{maxIter} \text{ || } |r|/|r^0| < \text{tolGCR}$ 
    return  $x$ 

```

---

#### IV. THE TECHNICAL CHALLENGE

The steady state response of our system could potentially be solved with direct LU decomposition or an indirect matrix implicit gradient conjugate residual method (GCR). LU decomposition would require computation of the Jacobian of

our system at each timestep. Although our system is sparsely connected, due to the wide band of our matrix a direct method would be inefficient. Instead we used matrix-implicit Newton-GCR to avoid the need to compute the Jacobian altogether. Additionally, this iterative method allows for early termination at a desired accuracy, reducing computation time.

Further, the dynamics of vortex formation and annihilation are the most important part of the system, so being able to quickly simulate long periods of time evolution with reasonable accuracy is crucial. Also, the lead-up to vortex formation can be very slow, but once a critical point is reached the vortices can form quite suddenly. Adaptive time step strategies allow us to simulate both regimes as quickly as is stable and accurate.

Therefore, for our technical challenge we implemented our trapezoidal simulator with an adaptive time step which used implicit-matrix Newton GCR for system solves.

To implement the adaptive time step, we simply check whether Newton-TGCR converges in our trapezoidal integrator. If it does, we continue to the next timestep. If it does not, we reduce the time step by an order of magnitude and try Newton again.

#### V. RESULTS

We compared the performance of our trapezoidal simulator to the standard forward Euler method. With both, we simulated vortex evolution for  $t_{stop} = 10$  in a  $20 \times 20 \times 3$  thin film initialized with  $\Psi = 1$  at each node and with an applied magnetic field of  $B_z = 0.5$ . Although each step of forward Euler is fast, the simulation becomes unstable for  $\Delta t > 10^{-3}$ . As a result, the fastest Forward Euler took 5352 seconds to run. Our trapezoidal simulator still functions with a timestep as large as  $\Delta t > 0.1$  and finishes in 86 seconds – sixty times faster. The RMSE between the two final computed statevectors was  $2.272 \times 10^{-4}$ , indicating good agreement.

Figure 2 shows a successful simulation of Abrikosov vortices formed by an applied magnetic field in a superconducting thin film, without periodic boundary conditions.

Figure 3a demonstrates the capability of our simulator to solve for dynamics in a three-dimensional cube of material large enough to sustain several vortex paths. Figure 3b shows vortex formation in a thin film with small  $h_x, h_y, h_z$  for higher resolution to better observe the shapes of the vortices. With  $h < 0.2$  convergence issues were encountered.

Figure 4a shows the computation time as a function of time step for a  $10 \times 10 \times 3$  grid. Note that Trapezoidal is faster than Forward Euler only for time steps larger than  $10^{-3}$ . Figure 4b shows how simulation time changes as grid size is increased. Note that run time increases quadratically with the scale of the sides of the thin film.

#### VI. TECHNICAL DISCUSSION

The difference between the results from a small-time-step forward Euler time evolution of our system and a large-time-step trapezoidal evolution are minor, especially since we care about vortex formation and trajectories rather than the exact

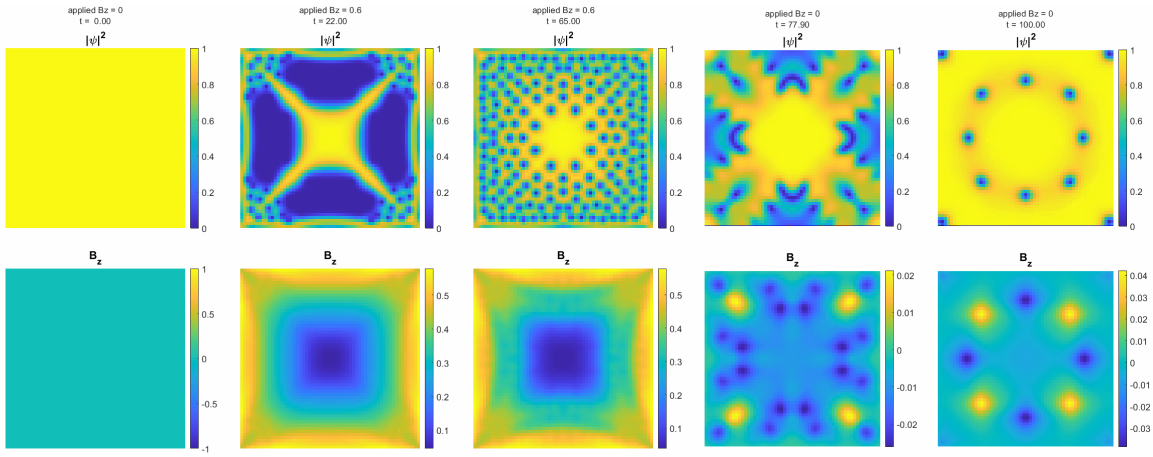


Fig. 2. Time evolution of a superconductor in a magnetic field. The top row shows the magnitude of the order parameter  $|\psi|^2$  while the bottom row shows the magnetic field in  $\hat{z}$ . At  $t = 0$  the magnetic field is off and the entire area is superconducting. At  $0 < t < 75$  A magnetic field  $B_z = 0.6$  is applied at the boundaries and vortex formation is observed. After the field is turned off, energy dissipates to the boundaries. In this dynamic state, vortex/anti-vortex (indicated by positive/magnetic fields) splitting can be observed in the corners. At steady state  $t = 100$  flux remains trapped in the superconductor. These figures were produced from a simulation of a  $60 \times 60 \times 3$  grid slice. Parameters:  $h_x = h_y = h_z = 1$ ,  $\kappa = 5$ ,  $d_x = d_y = d_z = 0$ .

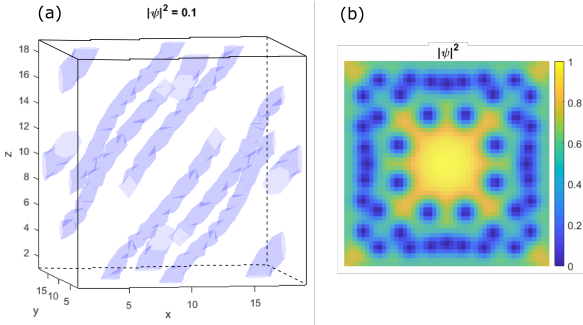


Fig. 3. (a) Vortex isosurfaces at  $|\psi|^2 = 0.1$ . A  $20 \times 20 \times 20$  cube was simulated with a diagonally applied magnetic field  $B_x = B_y = B_z = 0.4$ , ( $\kappa = 5$ ,  $h_x = h_y = h_z = 1$ ,  $d_x = d_y = d_z = 0$ ). (b) Vortex formation in a  $60 \times 60 \times 3$  plate with higher resolution ( $h_x = h_y = h_z = 0.5$ ) and  $\kappa = 3$ .

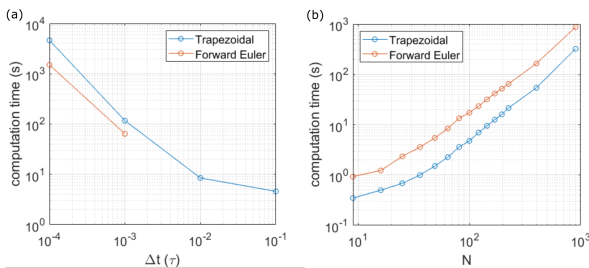


Fig. 4. (a) Computation time as a function of time step for a  $10 \times 10 \times 3$  grid. For each simulation  $t_{stop} = 4$  and final  $\Psi$  clearly shows vortex formation. (b) Computation time as a function of number of points. Each simulation used the maximum timestep for each method ( $\Delta t_{Trap} = 0.1$ ,  $\Delta t_{FE} = 0.001$  and  $t_{stop} = 1$ ).

value of the order parameter at each point in space. However, due to the large time step, trapezoidal can produce evolutions over long periods of time in minutes, while forward Euler can take over an hour to demonstrate even early stages of vortex formation in a  $20 \times 20 \times 3$  grid.

## VII. ETHICS & LIMITATIONS

Our simulation has some simplifications and limitations that could limit the accuracy of its predicted vortex dynamics. First, simulations of small thin films cannot necessarily be generalized to larger films, since edge effects can significantly impact vortex behavior. [6] Vortices deep in the bulk of a large block of superconducting material may behave differently, but due to size limitations such behaviors would be difficult to see with our simulator.

Furthermore, our simulator assumes a perfect superconducting material, free of impurities or defects. In reality such a material is impossible to achieve. In a real material, vortices can interact with impurities, resulting in different dynamics. [5] However, if someone were trying to control vortices for use in a superconducting device, such as fluxon-based quantum bits, [4] these kinds of larger-material or impurity-interaction behaviors could become significant to the circuit design choices. We would therefore recommend that our simulator only be used to see what kinds of vortex behaviors might be qualitatively expected, and that any conclusions be experimentally verified before being used in design decisions.

## VIII. CONCLUSIONS

We have created an adaptive time step, Jacobian-free, trapezoidal simulator for observing vortex dynamics in a type II superconductor. It produces qualitatively accurate simulations of these dynamics over long periods of time, much more quickly than could be achieved with forward Euler. We were able to observe complex vortex formation and annihilation dynamics during application of magnetic fields in thin films and 3-D blocks of superconducting materials.

## REFERENCES

- [1] On the theory of superconductivity. In D. Ter Haar, editor, *Collected Papers of L.D. Landau*, pages 546–568. Pergamon, 1965.

- [2] A. A. Abrikosov. The magnetic properties of superconducting alloys. *J. of Phys. Chem. Solids*, 2:199–208, 1957.
- [3] J. P. Allmaras. *Modeling and development of superconducting nanowire single-photon detectors*. PhD thesis, Caltech, 2020.
- [4] T. Golod, A. Iovan, and V. M. Krasnov. Single abrikosov vortices as quantized information bits. *Nature Communications*, 6, 2015.
- [5] S. Park, V. Barrena, S. Manas-Valero, and et al. Coherent coupling between vortex bound states and magnetic impurities in 2d layered superconductors. *Nature Communications*, 12, 2021.
- [6] B. L. T. Plourde, D. J. Van Harlingen, D. Y. Vodolazov, R. Besseling, M. B. S. Hesselberth, and P. H. Kes. Influence of edge barriers on vortex dynamics in thin weak-pinning superconducting strips. *Phys. Rev. B*, 64:014503, Jun 2001.
- [7] T. Winiecki and C. Adams. A fast semi-implicit finite-difference method for the tdgl equations. *Journal of Computational Physics*, 179(1):127–139, 2002.
- [8] R. Woo. China unveils 600 kph maglev train - state media. *Reuters*, Jul. 20, 2020 [Online].